Supporting Information

# As-Heteropentacenes: An Experimental and Computational Study on a Novel Class of Heteroacenes

Hiroaki Imoto,[a] Toshiki Fujii,[a] Susumu Tanaka,[a] Shunsuke Yamamoto,[b] Masaya Mitsuishi,[b] Takashi Yumura[c] and Kensuke Naka*[a]

[a] Faculty of Molecular Chemistry and Engineering, Graduate School of Science and Technology
Kyoto Institute of Technology
Goshokaido-cho, Matsugasaki, Sakyo-ku, Kyoto 606-8585, Japan
E-mail: kenaka@kit.ac.jp
[b] Institute of Multidisciplinary Research for Advanced Materials (IMRAM)
Tohoku University
2-1-1 Katahira, Aoba-ku, Sendai 980-8577, Japan
[c] Faculty of Materials Science and Engineering, Graduate School of Science and Technology
Kyoto Institute of Technology
Goshokaido-cho, Matsugasaki, Sakyo-ku, Kyoto 606-8585, Japan

**Table of Contents**

1. Materials
2. Measurement
3. X-ray crystallographic data for single crystalline products
4. Thin-film analysis
5. Synthesis
6. NMR spectra
7. Crystallographic data
8. Optical properties
9. Cyclic voltammetric analysis
10. XRD analysis
11. Computational study
12. Mechanism of [2+2] cycloaddition of **1**
13. Reference

## 1. Materials

Chloroform ($CHCl_3$), dichloromethane ($CH_2Cl_2$), methanol (MeOH), and copper(I) chloride (CuCl) were purchased from Nacalai Tesque, Inc. Superdehydrated tetrahydrofuran (stabilizer free) (THF), distilled water, *n*-butyllithium solution (1.6 M in hexane), diethyl ether ($Et_2O$), and magnesium sulfate anhydrous ($MgSO_4$), were purchased from Wako Pure Chemical Industry, Ltd. Diidophenylarsine,[1] 3,3'-diiodo-2,2'-bibenzofuran,[2] 3-iodo-2-(3-iodobenzo[*b*]thien-2-yl)benzofuran,[2] and 3,3'-dibromo-2,2'-bibenzo[*b*]thiophene[3] were prepared according to literature procedures.

## 2. Measurement

$^1$H- (400 MHz) and $^{13}$C{$^1$H}- (100 MHz) NMR spectra were recorded on a Bruker DPX-400 spectrometer. The samples were analyzed in $CDCl_3$ using $Me_4Si$ as an internal standard. The following abbreviations are used; s: singlet, d: doublet, t: triplet, m: multiplet. High-resolution mass spectra (HRMS) were obtained on a JEOL JMS-SX102A spectrometer. The UV−vis spectra were recorded on a Jasco spectrophotometer (V-670 KKN). Emission spectra were obtained on an FP-8500 instrument (JASCO), and absolute PL quantum yields ($\Phi$) were determined using a JASCO ILFC-847S instrument. Emission lifetimes were measured using Quantaurus-Tau (Hamamatsu Photonics).

## 3. X-ray crystallographic data for single crystalline products

The single crystal was mounted on a nylon loop. Intensity data were collected at room temperature on a Rigaku XtaLAB mini with graphite monochromated Mo Kα radiation. Readout was performed in the 0.073 mm pixel mode. The data were collected at room temperature to a maximum $2\theta$ value of 55.0°. Data were processed using the Crystal Clear program.[4] An empirical absorption correction[5] was applied. The data were corrected for Lorentz and polarization effects. The structure was solved by the direct method[6] and expanded using Fourier techniques. Non-hydrogen atoms were refined anisotropically. Hydrogen atoms were refined using the riding model. The final cycle of full-matrix least-squares refinement on $F^2$ was based on observed reflections and variable parameters. All calculations were performed using the CrystalStructure[7] crystallographic software package except for refinement, which was performed using SHELXL2013.[7] Crystal data and more information on X-ray data collection are summarized in Tables S1-7.

## 4. Thin-film analysis

The PMMA:**1**-**3** films were fabricated on patterned and UV-$O_3$ cleaned Si wafers (film XRD) and ITO substrates (SCLC measurements). Mixed solutions of PMMA and **1**-**3** in chlorobenzene (20:80 wt%) were spin-coated at a spin rate of 400 rpm (10 s) then 1000 rpm (60 s). The film XRD measurements were performed on SmartLab 3G (Rigaku) by Cu Kα radiation. For the SCLC devices, top Al electrodes (50 nm) were vacuum deposited (VKS-200, Osaka Vacuum) at a base pressure of $7 \times 10^{-4}$ Pa through shadow masks. The *J*-*V* curves were measured by a semiconductor parameter analyzer (4155C, Agilent) in a vacuum probe station. The film thickness was determined by AFM (SPA-400, SII Inc.).

## 5. Synthesis

***Note***

Low molecular weight organoarsenic compounds have volatility, and it is necessary to avoid the procedures generating volatile organoarsenic compounds. For safety, experiments should be performed in a fume food. Besides, in a few cases, spontaneously flammable compounds are obtained as described in the literature if one tries to synthesize alkyl arsine derivatives,[8] and thus fire prevention measures should be taken.

*11-Phenyl-11H-arsolo[3,2-b:4,5-b']bis[1]benzofuran (**1**)*

1.6 M *n*-hexane solution of *n*-BuLi (1.4 mL, 2.24 mmol, 2.3 eq) was added dropwise to a THF/$Et_2O$ mixed solution (THF: 23 mL, $Et_2O$: 23 mL) of 3,3'-diiodo-1,1'-bibenzofuran (0.478 g, 0.982 mmol, 1.0 eq) at -100 °C under $N_2$ atmosphere and the mixture was stirred at that temperature for 30 min. CuCl (0.214 g, 2.17 mmol, 2.2 eq) was added in one portion, and the reaction mixture was stirred at that temperature for 30 min. Then, separately prepared diiodophenylarsine (1.1 eq) was added dropwise into the mixture. The mixture was heated to 40 °C and stirring for 30 min. Distilled water (15 mL) was poured into the reaction mixture, and the organic layer was concentrated in vacuo. The aqueous layer was extracted with $CHCl_3$, and the combined organic phase was dried over $MgSO_4$, filtered and concentrated under reduced pressure. The residue was purified through the silica column chromatography (eluent: hexane). The title compound was obtained as a light yellow solid (31%, 118 mg, 0.308 mmol). Single crystals of **1** were obtained by slow evaporation of saturated solution in $CH_2Cl_2$. Crystals *α*-**1** and β-**1** were separated by hand with checking the emission color

under UV-irradiation.[9] During the examination of X-ray crystallography, a crystal of [2+2] cycloadduct of **1** was found, but the amount was too small to perform NMR spectroscopy.
$^1$H-NMR (acetone-$d_6$, 400 MHz): $\delta$ 7.82 (d, $J$ = 6.9 Hz, 2H), 7.71 (d, $J$ = 7.4 Hz, 2H), 7.60-7.57 (m, 2H), 7.42-7.33 (m. ,4H), 7.31-7.29 (m, 3H) ppm; $^{13}$C{$^1$H}-NMR (acetone-$d_6$, 100 MHz): $\delta$ 159.1, 153.8, 136.8, 133.2, 133.1, 130.0, 130.0, 125.9, 125.8, 125.2, 121.4, 113.2 ppm. HR-FAB-MS (m/z): calculated for $C_{22}H_{13}O_2As$ $[M]^+$: 384.0132; found: 384.0128.

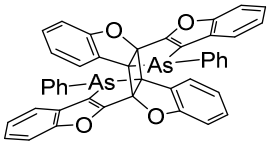


**Chart S1.** Chemical structure of [2+2] cycloadduct of **1**.

*[1]Benzofurano[2',3':4,5]arsolo[3,2-b][1]benzothiophene (**2**)*
1.6 M *n*-hexane solution of *n*-BuLi (1.2 mL, 1.92 mmol, 2.2 eq) was added dropwise to a THF/$Et_2O$ mixed solution (THF: 10 mL, $Et_2O$: 40 mL) of 3-iodo-2-(3-iodobenzo[b]thien2-yl)-benzofuran (0.438 g, 0.873 mmol, 1.0 eq) at -100 °C under $N_2$ atmosphere and the mixture was stirred at that temperature for 1 hour. CuCl (0.190 g, 1.92 mmol, 2.2 eq) was added in one portion, and the reaction mixture was stirred at that temperature for 1 hour. Then, separately prepared diiodophenylarsine (1.1 eq) was added dropwise into the mixture. The mixture was heated to 30 °C and stirring for 1 hour. Distilled water (15 mL) was poured into the reaction mixture, and the organic layer was concentrated in vacuo. The aqueous layer was extracted with $CHCl_3$, and the combined organic phase was dried over $MgSO_4$, filtered and concentrated under reduced pressure. The residue was purified through the silica column chromatography (eluent: hexane). The title compound was obtained as a light yellow solid (24%, 84.1 mg, 0.169 mmol). Single crystals of **2** were obtained by slow evaporation of saturated solution in $CH_2Cl_2$.
$^1$H-NMR (acetone-$d_6$, 400 MHz): $\delta$ 8.09 (d, $J$ = 7.8 Hz, 1H), 7.96 (d, $J$ = 6.9 Hz, 1H), 7.79 (d, $J$ = 6.9 Hz, 1H), 7.70 (d, $J$ = 7.4 Hz, 1H), 7.56-7.53 (m, 2H), 7.48-7.32 (m, 4H), 7.29-7.26 (m, 3H) ppm; $^{13}$C{$^1$H}-NMR (acetone-$d_6$, 100 MHz): $\delta$ 160.3, 158.2, 145.2, 142.7, 139.2, 136.3, 135.8, 132.4, 129.4, 129.1, 129.1, 125.3, 124.5, 124.2, 123.9, 123.6, 122.8, 122.4, 120.4, 112.2 ppm; HR FAB-MASS:(m/z): calculated for $C_{22}H_{13}OSAs$ $[M+H]^+$: 400.9984 found: 400.9981.

*11-Phenyl-11H-arsolo[3,2-b:4,5-b']bis[1]benzothiophene (**3**)*
1.6 M *n*-hexane solution of *n*-BuLi (1.3 mL, 2.08 mmol, 2.2 eq) was added dropwise to a THF/$Et_2O$ mixed solution (THF: 10 mL, $Et_2O$: 40 mL) of 3,3'-dibromo-2,2'-bibenzo[*b*]thiophene (0.402 g, 0.948 mmol, 1.0 eq) at -78 °C under $N_2$ atmosphere and the mixture was stirred at that temperature for 1 hour. CuCl (0.209 g, 2.11 mmol, 2.2 eq) was added in one portion, and the reaction mixture was stirred at that temperature for 1 hour. Then, separately prepared diiodophenylarsine (1.1 eq) was added dropwise into the mixture. The mixture was heated to 30 °C and stirring for 1 hour. Distilled water (15 mL) was poured into the reaction mixture, and the organic layer was concentrated in vacuo. The aqueous layer was extracted with $CHCl_3$, and the combined organic phase was dried over $MgSO_4$, filtered and concentrated under reduced pressure. The residue was purified through the silica column chromatography (eluent: hexane). The title compound was obtained as a yellow solid (36%, 141 mg, 0.337 mmol). Single crystals of **3** were obtained by slow evaporation of saturated solution in $CH_2Cl_2$.
$^1$H-NMR (acetone-$d_6$, 400 MHz): $\delta$ 8.09 (d, $J$ =7.4 Hz, 2H), 7.92 (d, $J$ = 7.0 Hz, 2H), 7.50-7.39 (m, 6H), 7.28-7.26 (m, 3H) ppm; $^{13}$C{$^1$H}-NMR (acetone-$d_6$, 100 MHz): $\delta$ 144.5, 143.0, 139.3, 136.8, 132.5, 131.4, 129.1, 129.1, 125.3, 124.4, 123.5, 122.8 ppm; HR FAB-MASS:(m/z): calculated for $C_{22}H_{13}S_2As$ $[M]^+$: 415.9675; found: 415.9681.

## 6. NMR spectra

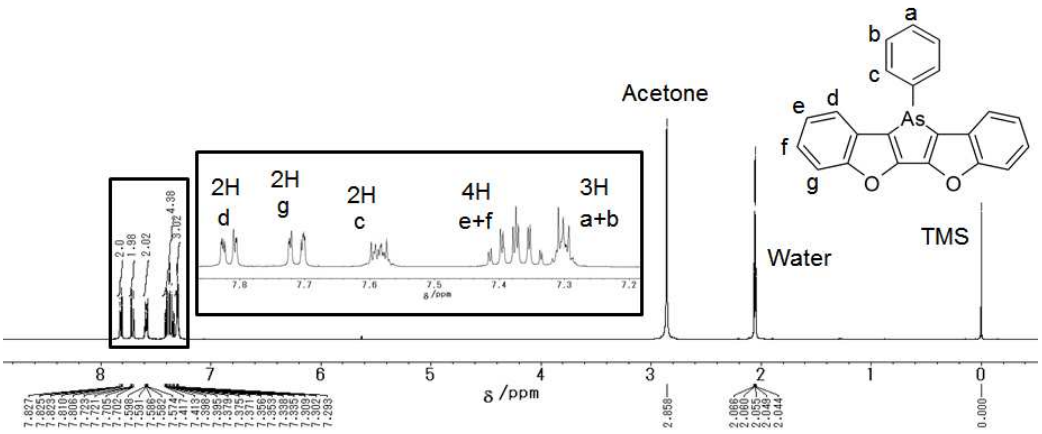


**Figure S1.** $^{1}$H-NMR spectrum (400 MHz) of **1** in acetone-$d_6$.

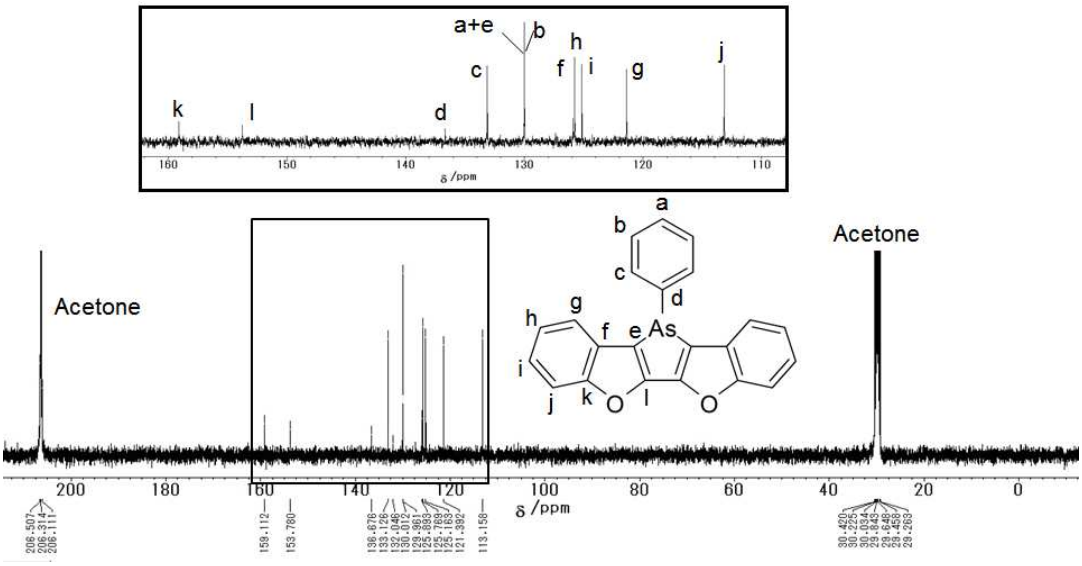


**Figure S2.** $^{13}$C{$^{1}$H}-NMR spectrum (100 MHz) of **1** in acetone-$d_6$.

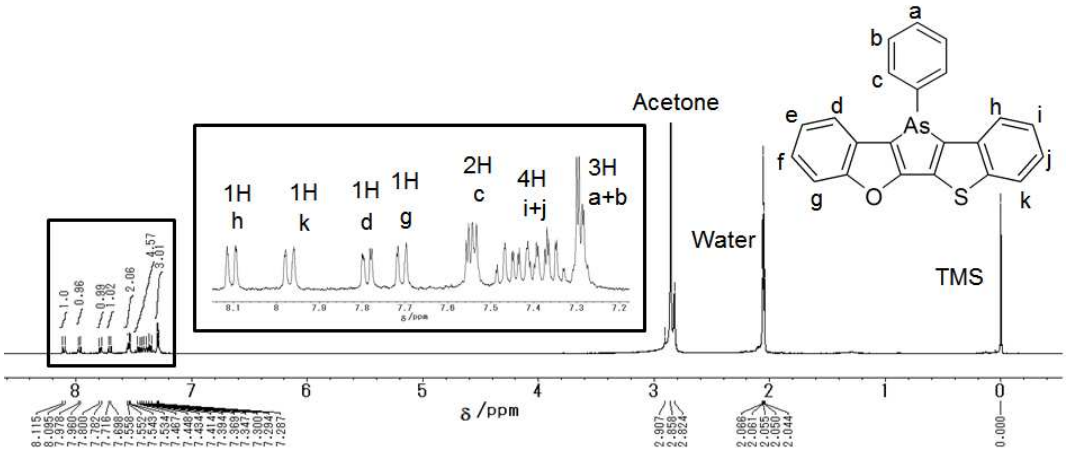


**Figure S3.** $^{1}$H-NMR spectrum (400 MHz) of **2** in acetone-$d_6$.

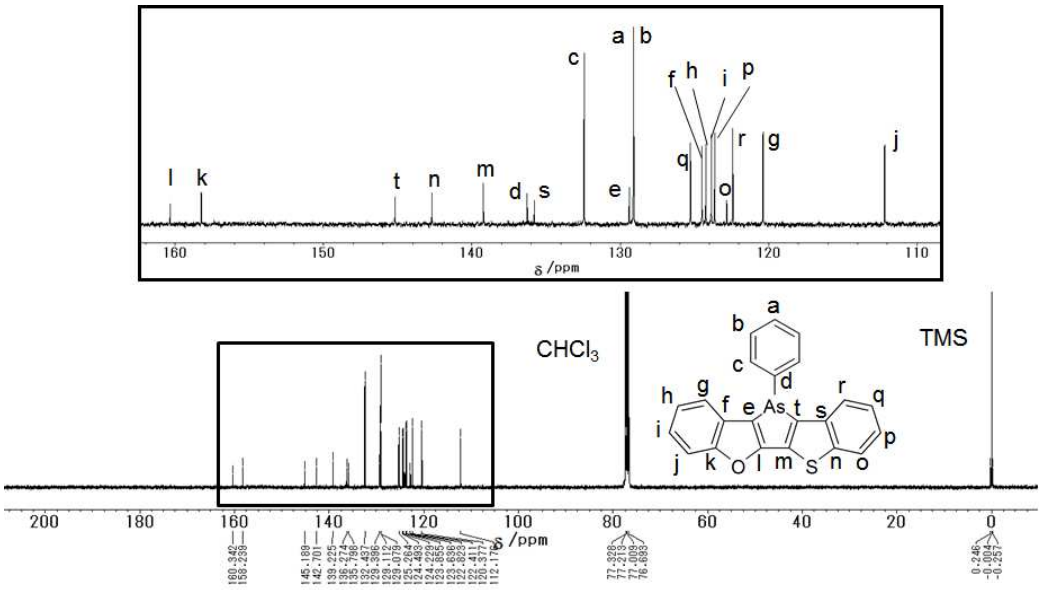


**Figure S4.** $^{13}$C{$^{1}$H}-NMR spectrum (400 MHz) of **2** in $CDCl_3$.

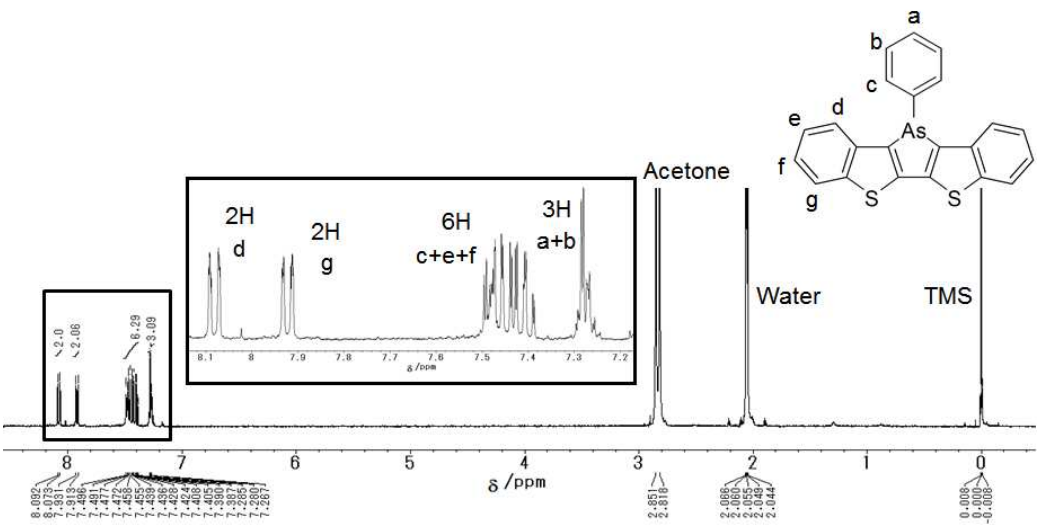


**Figure S5.** $^{1}$H-NMR spectrum (400 MHz) of **3** in acetone-$d_6$.

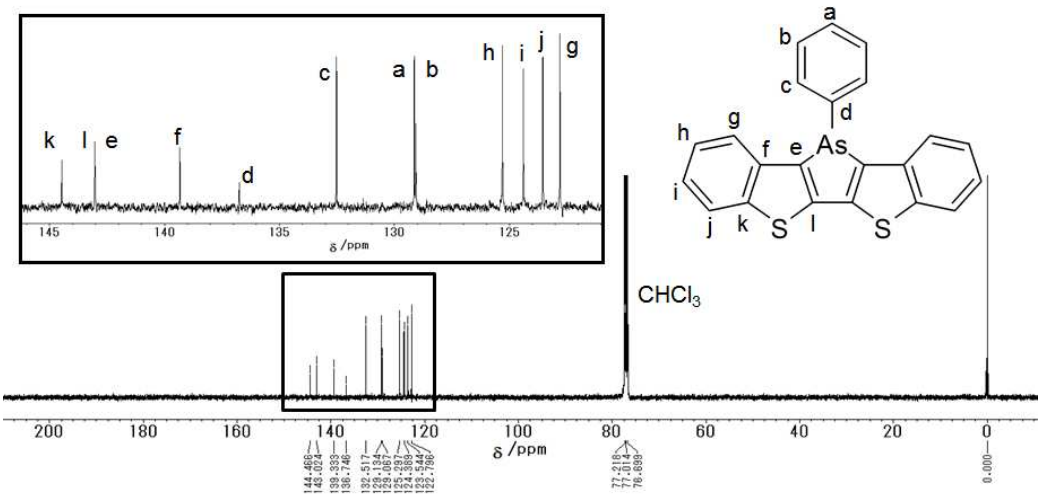


**Figure S6.** $^{13}$C{$^{1}$H}-NMR spectrum (400 MHz) of **3** in $CDCl_3$.

## 7. Crystallographic data

**Table S1**. Crystallographic data of *α*-**1**, *β*-**1**, and [2+2] cycloadduct of **1**

| | *α*-**1** | *β*-**1** | [2+2] cycloadduct of **1** |
|---|---|---|---|
| Crystal data | | | |
| Experimental Formula | $C_{22}H_{13}AsO_2$ | $C_{22}H_{13}AsO_2$ | $C_{44}H_{26}As_2O_4$ |
| Formula Weight | 384.27 | 384.27 | 768.53 |
| Crystal Dimension, $mm^3$ | 0.250 × 0.180 × 0.160 | 0.430 × 0.420 × 0.180 | 0.370 ×0.100 ×0.080 |
| Crystal System | monoclinic | monoclinic | triclinic |
| Space Group | Pc | $P2_1/n$ | P-1 |
| a, Å | 5.406(5) | 11.252(7) | 12.9971(2) |
| b, Å | 15.925(13) | 8.158(5) | 15.3555(6) |
| c, Å | 9.741(8) | 18.139(12) | 17.0719(4) |
| α, deg | - | - | 61.514(11) |
| β, deg | 100.852(11) | 96.437(6) | 71.046(11) |
| γ, deg | - | - | 74.388(13) |
| Volume, $Å^3$ | 823.6(12) | 1654.5(18) | 2805.4(3) |
| $D_{calcd}$, g $cm^{-3}$ | 1.549 | 1.543 | 1.365 |
| Z | 2 | 4 | 3 |
| F(000) | 388.00 | 776.00 | 1164.00 |
| Data Collection | | | |
| Temperature, deg | 25.0 | 25.0 | 25.0 |
| 2*θ*max, deg | 54.9 | 55.0 | 55.0 |
| Tmin/Tmax | 0.591 – 0.717 | 0.557 – 0.689 | 0.771 – 0.864 |
| Refinement | | | |
| No. of Observed Data | 3700 | 3793 | 12806 |
| No. of Parameters | 226 | 226 | 676 |
| R1[a], wR2[b] | 0.1189, 0.2954 | 0.0355, 0.0960 | 0.0568, 0.1652 |
| Goodness of Fit Indicator | 1.260 | 1.081 | 1.027 |

[a]$R1 = \Sigma \mid |Fo| - |Fc| \mid / \Sigma |Fo|$ [b]$wR2 = [\ \Sigma\ w\ ((Fo^2-Fc^2)^2 / \Sigma\ w\ (Fo^2)^2\ ]^{1/2}$ $w = [\ \sigma^2(Fo^2)\ ]^{-1}$

CCDC # 1847197 (*α*-**1**), 1847200 (*β*-**1**), and 1852784 ([2+2] cycloadduct of **1**).

**Table S2**. Crystallographic data of **2** and **3**

| | **2** | **3** |
|---|---|---|
| Crystal data | | |
| Experimental Formula | $C_{22}H_{13}AsOS$ | $C_{22}H_{13}AsS_2$ |
| Formula Weight | 400.33 | 416.39 |
| Crystal Dimension, $mm^3$ | 0.200 × 0.200 × 0.200 | 0.350 × 0.090 × 0.040 |
| Crystal System | Monoclinic | monoclinic |
| Space Group | $P2_1/n$ | $P2_1$ |
| a, Å | 10.22(3) | 11.852(3) |
| b, Å | 10.58(3) | 6.2399(11) |
| c, Å | 16.79(5) | 13.179(3) |
| α, deg | - | - |
| β, deg | 90.58(4) | 113.019(9) |
| γ, deg | - | - |
| Volume, $Å^3$ | 1815(9) | 897.0(3) |
| $D_{calcd}$, g $cm^{-3}$ | 1.465 | 1.541 |
| Z | 4 | 2 |
| F(000) | 808.00 | 420.00 |
| Data Collection | | |
| Temperature, deg | 25.0 | 25.0 |
| 2*θ*max, deg | 54.6 | 55.0 |
| Tmin/max | 0.600 – 0.671 | 0.718 – 0.918 |
| Refinement | | |
| No. of Observed Data | 4007 | 4094 |
| No. of Parameters | 226 | 226 |
| R1[a], wR2[b] | 0.0677, 0.1901 | 0.0377, 0.0630 |
| Goodness of Fit Indicator | 1.052 | 0.995 |

[a]$R1 = \Sigma \mid |Fo| - |Fc| \mid / \Sigma |Fo|$ [b]$wR2 = [\ \Sigma\ w\ ((Fo^2-Fc^2)^2 / \Sigma\ w\ (Fo^2)^2\ ]^{1/2}$ $w = [\ \sigma^2(Fo^2)\ ]^{-1}$

CCDC # 1847199 (**2**) and 1847197 (**3**)

**Table S3.** ORTEP drawing (ellipsoids at 50% probability), selected angles (deg) and distances (Å) of *α*-**1**.

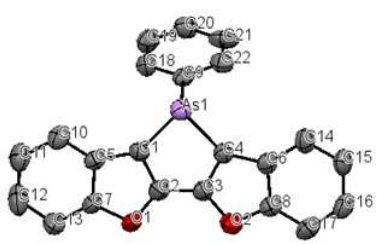


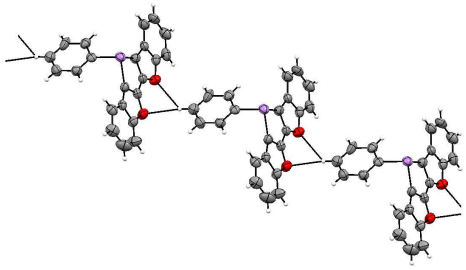

| interplanar angle (°)[a] | | angle (°) | |
|---|---|---|---|
| O(1)C(2)C(1)C(5)C(7)-O(2)C(3)C(4)C(6)C(8) | 3.97 | C(1)-As(1)-C(4) | 85.9(6) |
| | | C(1)-As(1)-C(9) | 97.7(6) |
| C(5)C(7)C(13)C(12)C(11)C(10)-C(6)C(8)C(17)C(16)C(15)C(14) | 3.21 | C(4)-As(1)-C(9) | 98.9(6) |
| | | As(1)-C(1)-C(5) | 143.6(9) |
| distance (Å) | | As(1)-C(4)-C(6) | 143.8(11) |
| As(1)-C(1) | 1.948(14) | As(1)-C(1)-C(2) | 109.7(10) |
| As(1)-C(4) | 1.960(14) | As(1)-C(4)-C(3) | 109.4(10) |
| As(1)-C(9) | 1.978(15) | C(1)-C(2)-C(3) | 116.9(13) |
| O(1)-C(2) | 1.354(19) | C(2)-C(3)-C(4) | 117.6(12) |
| O(1)-C(7) | 1.378(17) | O(1)-C(2)-C(1) | 113.3(12) |
| O(2)-C(3) | 1.376(17) | C(2)-C(1)-C(5) | 105.9(12) |
| O(2)-C(8) | 1.39(2) | C(1)-C(5)-C(7) | 104.4(11) |
| C(1)-C(2) | 1.389(18) | O(1)-C(7)-C(5) | 111.1(12) |
| C(2)-C(3) | 1.39(2) | C(2)-O(1)-C(7) | 105.0(10) |
| C(3)-C(4) | 1.38(2) | O(2)-C(3)-C(4) | 112.3(13) |
| C(1)-C(5) | 1.43(2) | C(3)-C(4)-C(6) | 105.9(12) |
| C(5)-C(7) | 1.435(18) | C(4)-C(6)-C(8) | 106.4(12) |
| C(4)-C(6) | 1.42(2) | O(2)-C(8)-C(6) | 110.4(12) |
| C(6)-C(8) | 1.401(19) | C(3)-O(2)-C(8) | 104.9(11) |

[a]Angles between mean planes.

**Table S4.** ORTEP drawing (ellipsoids at 50% probability), selected angles (deg) and distances (Å) of *β*-**1**.

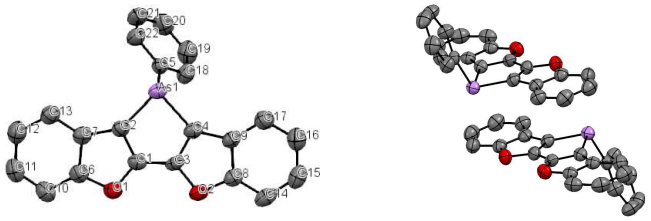

| interplanar angle (°)[a] | | angle (°) | |
|---|---|---|---|
| O(1)C(1)C(2)C(7)C(6)-O(2)C(3)C(4)C(9)C(8) | 2.66 | C(2)-As(1)-C(4) | 84.97(11) |
| | | C(2)-As(1)-C(5) | 100.36(11) |
| C(7)C(6)C(10)C(11)C(12)C(13)-C(9)C(8)C(14)C(15)C(16)C(17) | 1.96 | C(4)-As(1)-C(5) | 101.00(10) |
| | | As(1)-C(2)-C(7) | 144.00(19) |
| distance (Å) | | As(1)-C(4)-C(9) | 143.26(18) |
| As(1)-C(2) | 1.959(3) | As(1)-C(2)-C(1) | 110.14(19) |
| As(1)-C(4) | 1.956(3) | As(1)-C(4)-C(3) | 109.63(18) |
| As(1)-C(5) | 1.958(2) | C(2)-C(1)-C(3) | 117.0(2) |
| O(1)-C(1) | 1.368(3) | C(1)-C(3)-C(4) | 117.6(2) |
| O(1)-C(6) | 1.385(3) | O(1)-C(1)-C(2) | 114.0(2) |
| O(2)-C(3) | 1.385(3) | C(1)-C(2)-C(7) | 105.2(2) |
| O(2)-C(8) | 1.390(3) | C(2)-C(7)-C(6) | 105.5(2) |
| C(1)-C(2) | 1.366(3) | O(1)-C(6)-C(7) | 111.2(2) |
| C(1)-C(3) | 1.388(4) | C(1)-O(1)-C(6) | 104.08(18) |
| C(3)-C(4) | 1.374(3) | O(2)-C(3)-C(4) | 111.7(2) |
| C(2)-C(7) | 1.436(4) | C(3)-C(4)-C(9) | 106.4(2) |
| C(6)-C(7) | 1.407(3) | C(4)-C(9)-C(8) | 105.7(2) |
| C(4)-C(9) | 1.439(4) | O(2)-C(8)-C(9) | 110.8(2) |
| C(8)-C(9) | 1.398(3) | C(3)-O(2)-C(8) | 105.34(18) |

[a]Angles between mean planes.

**Table S5.** ORTEP drawing (ellipsoids at 50% probability), selected angles (deg) and distances (Å) of **2**.

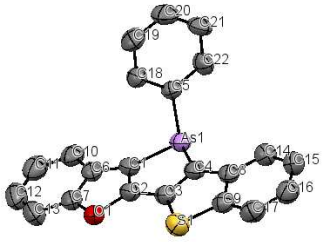


| interplanar angle (°)[a] | | angle (°) | |
|---|---|---|---|
| O(1)C(2)C(1)C(6)C(7)-S(1)C(3)C(4)C(5)C(9) | 2.25 | C(1)-As(1)-C(4) | 84.9(3) |
| | | C(1)-As(1)-C(5) | 101.9(3) |
| C(6)C(7)C(13)C(12)C(11)C(10)-C(8)C(9)C(17)C(16)C(15)C(14) | 2.88 | C(4)-As(1)-C(5) | 101.9(3) |
| | | As(1)-C(1)-C(6) | 142.3(4) |
| distance (Å) | | As(1)-C(4)-C(8) | 136.2(4) |
| As(1)-C(1) | 1.959(7) | As(1)-C(1)-C(2) | 111.0(4) |
| As(1)-C(4) | 1.964(8) | As(1)-C(4)-C(3) | 111.9(4) |
| As(1)-C(5) | 1.979(7) | C(1)-C(2)-C(3) | 117.9(5) |
| O(1)-C(2) | 1.461(7) | C(2)-C(3)-C(4) | 113.9(5) |
| O(1)-C(7) | 1.450(8) | O(1)-C(2)-C(1) | 115.3(5) |
| S(1)-C(3) | 1.748(7) | C(2)-C(1)-C(6) | 106.1(5) |
| S(1)-C(9) | 1.752(7) | C(1)-C(6)-C(7) | 106.5(5) |
| C(1)-C(2) | 1.353(8) | O(1)-C(7)-C(6) | 112.4(5) |
| C(2)-C(3) | 1.455(9) | C(2)-O(1)-C(7) | 99.7(4) |
| C(3)-C(4) | 1.380(8) | S(1)-C(3)-C(4) | 114.7(4) |
| C(1)-C(6) | 1.447(8) | C(3)-C(4)-C(8) | 111.7(5) |
| C(6)-C(7) | 1.415(9) | C(4)-C(8)-C(9) | 111.1(5) |
| C(4)-C(8) | 1.442(9) | S(1)-C(9)-C(8) | 112.7(5) |
| C(8)-C(9) | 1.431(9) | C(3)-S(1)-C(9) | 89.7(3) |

[a]Angles between mean planes.

**Table S6.** ORTEP drawing (ellipsoids at 50% probability), selected angles (deg) and distances (Å) of **3**.

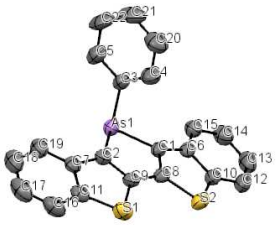

| interplanar angle (°)[a] | | angle (°) | |
|---|---|---|---|
| S(1)C(9)C(2)C(7)C(11)-S(2)C(8)C(1)C(6)C(10) | 10.36 | C(1)-As(1)-C(2) | 85.61(19) |
| | | C(1)-As(1)-C(3) | 101.9(2) |
| C(11)C(7)C(19)C(18)C(17)C(16)-C(10)C(6)C(15)C(14)C(13)C(12) | 13.97 | C(2)-As(1)-C(3) | 99.0(2) |
| | | As(1)-C(2)-C(7) | 135.4(4) |
| distance (Å) | | As(1)-C(1)-C(6) | 134.7(4) |
| As(1)-C(1) | 1.942(4) | As(1)-C(2)-C(9) | 111.3(3) |
| As(1)-C(2) | 1.946(5) | As(1)-C(1)-C(8) | 111.3(3) |
| As(1)-C(3) | 1.954(5) | C(2)-C(9)-C(8) | 115.4(4) |
| S(1)-C(9) | 1.732(5) | C(1)-C(8)-C(9) | 116.1(4) |
| S(1)-C(11) | 1.738(5) | S(1)-C(9)-C(2) | 113.5(3) |
| S(2)-C(8) | 1.734(4) | C(7)-C(2)-C(9) | 112.6(5) |
| S(2)-C(10) | 1.745(5) | C(2)-C(7)-C(11) | 110.8(4) |
| C(2)-C(9) | 1.370(7) | S(1)-C(11)-C(7) | 112.4(3) |
| C(8)-C(9) | 1.454(6) | C(9)-S(1)-C(11) | 90.7(2) |
| C(1)-C(8) | 1.366(7) | S(2)-C(8)-C(1) | 113.8(3) |
| C(2)-C(7) | 1.438(6) | C(6)-C(1)-C(8) | 112.5(4) |
| C(7)-C(11) | 1.415(8) | C(1)-C(6)-C(10) | 111.4(4) |
| C(1)-C(6) | 1.434(6) | S(2)-C(10)-C(6) | 111.7(3) |
| C(6)-C(10) | 1.421(7) | C(8)-S(2)-C(10) | 90.7(2) |

[a]Angles between mean planes.

**Table S7.** ORTEP drawing (ellipsoids at 50% probability), distances (Å) and selected angles (deg) of [2+2] cycloadduct of **1**.

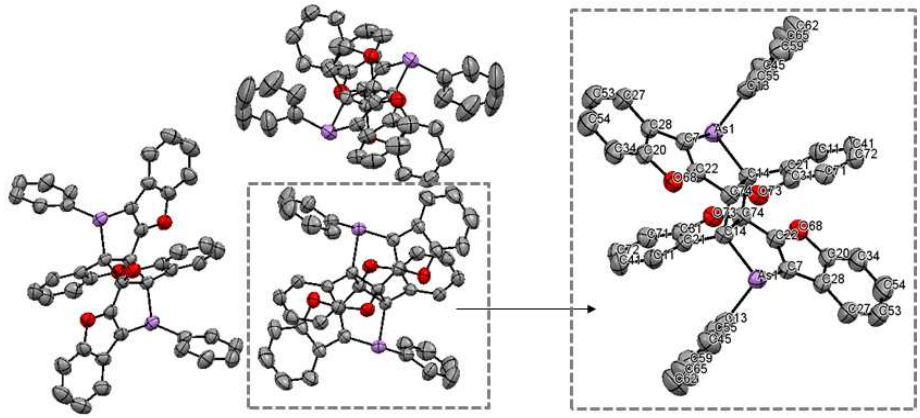

| distance (Å) | | angle (°) | |
|---|---|---|---|
| As(1)-C(7) | 1.938(6) | C(7)-As(1)-C(14) | 86.0(2) |
| As(1)-C(14) | 2.034(5) | C(7)-As(1)-C(13) | 102.6(2) |
| As(1)-C(13) | 1.954(5) | C(13)-As(1)-C(14) | 98.6(2) |
| C(14)-C(74) | 1.562(6) | As(1)-C(14)-C()74 | 109.4(3) |
| C(14)-C(74) | 1.584(5) | C(14)-C(74)-C(22) | 109.0(4) |
| C(7)-C(22) | 1.351(6) | C(74)-C(14)-C(74) | 89.0(3) |
| O(68)-C(22) | 1.374(7) | C(14)-C(74)-C(14) | 91.0(3) |
| O(68)-C(20) | 1.388(8) | C(74)-C(22)-C(7) | 121.9(4) |
| O(73)-C(31) | 1.389(7) | C(22)-C(7)-As(1) | 113.4(4) |
| O(73)-C(74) | 1.443(5) | C(7)-C(22)-O(68) | 114.1(4) |
| C(20)-C(28) | 1.409(7) | C(22)-O(68)-C(20) | 104.4(4) |
| C(7)-C(28) | 1.460(9) | O(68)-C(20)-C(28) | 111.3(5) |
| C(21)-C(31) | 1.387(7) | C(20)-C(28)-C(7) | 104.6(5) |
| C(14)-C(21) | 1.498(8) | C(28)-C(7)-C(22) | 105.6(4) |
| C(22)-C(74) | 1.467(8) | C(14)-C(74)-O(73) | 108.8(3) |
| | | C(74)-O(73)-C(31) | 106.6(3) |
| | | O(73)-C(31)-C(21) | 114.1(4) |
| | | C(31)-C(21)-C(14) | 108.9(4) |
| | | C(21)-C(14)-C(74) | 101.6(4) |

## 8. Optical properties

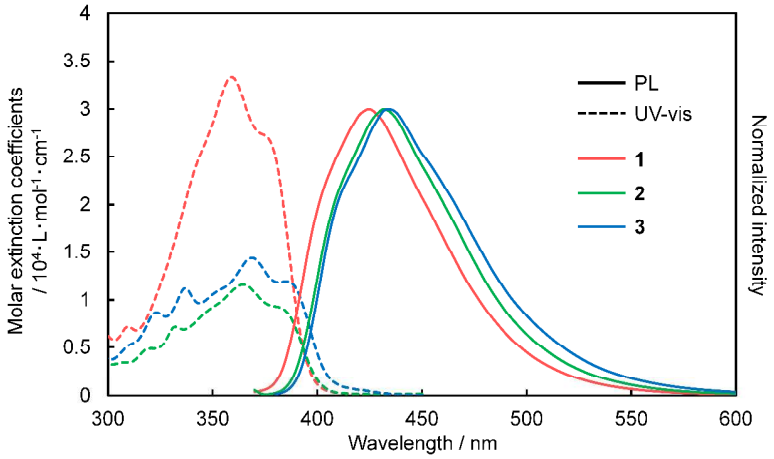


**Figure S7**. UV-vis absorption and photoluminescence spectra of **1**, **2**, and **3** in $CHCl_3$ solution ($1.0 \times 10^{-5}$ M).

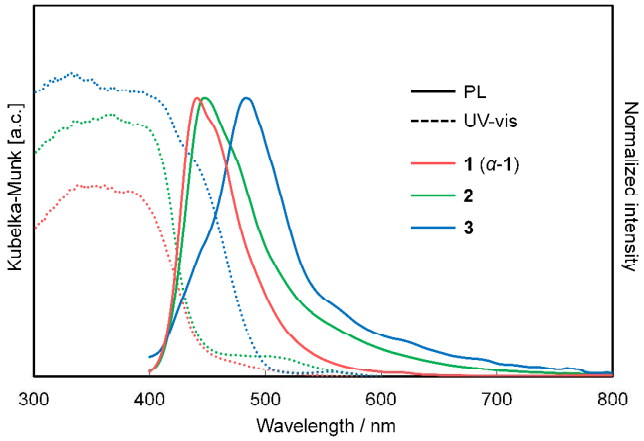


**Figure S8**. UV-vis absorption and photoluminescence spectra of **1**, **2**, and **3** in the solid-state.

**Table S8.** Optical properties of $\alpha$-**1**, $\beta$-**1**, and 5 wt% PMMA film of **1**.

| Polymorphs | $\lambda_{ex}$ [nm][b] | $\lambda_{em}$ [nm][c] | $\Phi$[d] |
|---|---|---|---|
| $\alpha$-**1** | 416 | 441 | 0.18 |
| $\beta$-**1** | 412 | 465 | 0.39 |
| 5 wt% PMMA film of **1**[a] | 411 | 460 | 0.16 |

[a]Prepared by drop-cast onto a silicon substrate from a chloroform solution (PMMA: 80 g/L, **1**: 4 g/L). [b]Excitation maximum (emission at the $\lambda_{em}$). [c]Emission maximum (excitation at the $\lambda_{ex}$). [d]Absolute quantum yield.

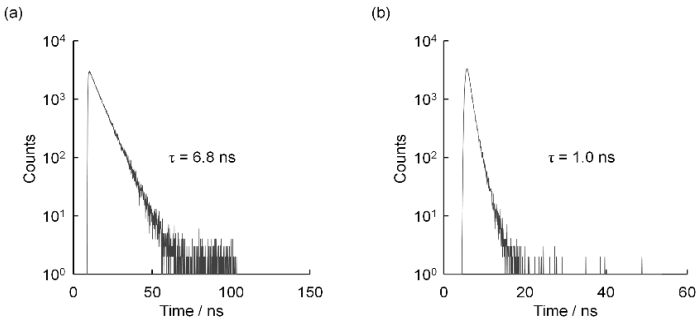


**Figure S9**. The emission decay kinetics of (a) $\alpha$-**1**, and (b) **2** in the solid-state on excitation at 365 and 405 nm, respectively.

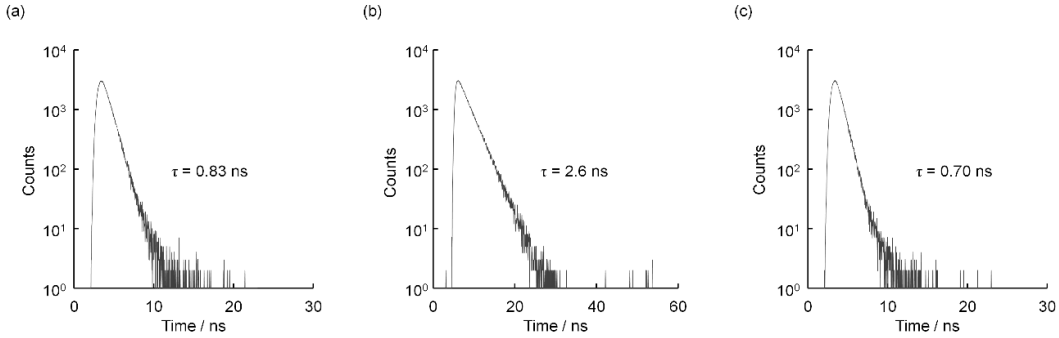


**Figure S10**. The emission decay kinetics of (a) **1**, (b) **2**, and (c) **3** in THF solution ($c$ = $10^{-4}$ M) on excitation at 365 nm.

## 9. Cyclic voltammetric analysis

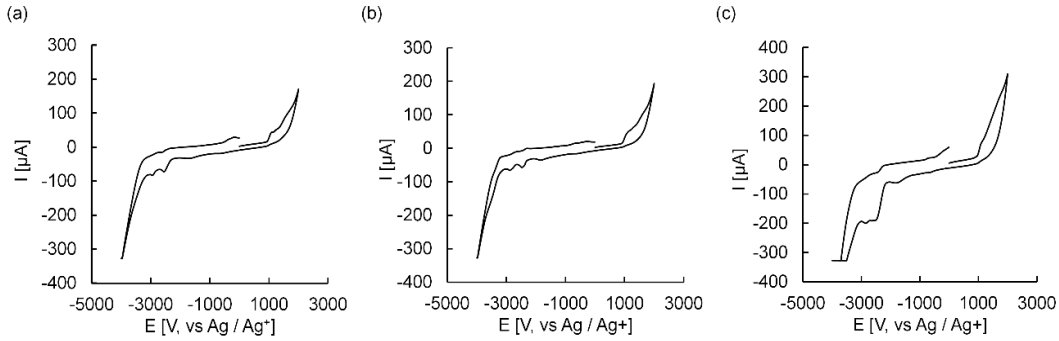


**Figure S11.** Cyclic voltammograms of (a) **1**, (b) **2**, and **3** measured in THF solution ($c$ = 0.1 M) at the scan rate of 100 mV/s under $N_2$. The working electrode was a glassy carbon, the counter electrode was a platinum wire, and the reference electrode was an $Ag^0$ / $Ag^+$.

**Table S9.** Electronic properties of **1**, **2** and **3**.

| | CV | | | DFT calculation[d] | | | |
|---|---|---|---|---|---|---|---|
| | HOMO [eV][a] | LUMO [eV][b] | $E_g$ [eV][c] | HOMO [eV][e] | LUMO [eV][e] | $E_g$ [eV][f,g] | $f$[f,h] |
| **1** | -5.55 | -2.31 | 3.24 | -5.56 | -1.82 | 3.37 | 0.5366 |
| **2** | -5.56 | -2.30 | 3.26 | -5.58 | -1.90 | 3.29 | 0.4633 |
| **3** | -5.59 | -2.44 | 3.15 | -5.59 | -1.96 | 3.24 | 0.3941 |

[a] $E$(HOMO) = −($E_{ox}$ + 4.80) [eV], where $E_{ox}$ is the onset potential of oxidation, observed in the CV analyses. [b] E(LUMO) = −($E_{red}$ + 4.80) [eV], where $E_{red}$ is the onset potential of reduction, observed in the CV analyses. [c] $E_g$ = $E$ (LUMO) – $E$(HOMO) [eV]. [d] Structures were optimized by DFT calculation, and all calculations were performed at the B3LYP/6-31G+(d,p) level of theory. [e] DFT calculation. [f] TD-DFT calculation. [g] Energy of HOMO-LUMO transition. [h] Oscillator strength of HOMO-LUMO transition.

## 10. XRD analysis

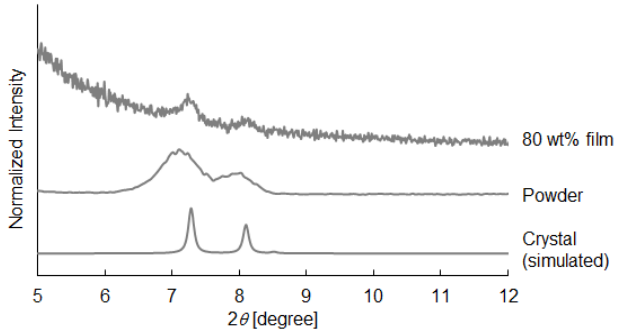


**Figure S12.** XRD patterns of **3**: 80 wt% film in PMMA (measured), powder (measured), and crystal (simulated).

## 11. Computational study

***Computational methods***

Density functional theory (DFT) calculations were carried out to investigate the frontier orbitals of the synthesized compounds. In addition, the vertical excitation energies ($\Delta E$) and oscillator strengths ($f$) were obtained for the three lowest S0 → S1 transitions at the optimized ground state equilibrium geometries by using the time-dependent density functional theory (TD-DFT). These calculations employed B3LYP/6-31G+(d,p).

Nucleus-independent chemical shift (NICS) values were calculated by GIAO-B3LYP/6-311G+(d,p) based on the optimized structures shown in Table S10-12. $NICS(1)_{zz}$ values were employed for the evaluation of aromaticity; the ring centers of the arsole rings were determined by the average of the coordinates of atoms 1-5 in Tables S10-12.

To understand the formation of [2+2] cycloadduct obtained in the X-ray crystallography, B3LYP/6-31G(d,p) calculations were employed. To obtain the energy profile, local minima, corresponding to reactants, intermediates, and products, as well as saddle points, corresponding to transition states, were obtained in Figure S14. Harmonic vibrational frequencies were systematically computed to confirm that each optimized geometry corresponds to a local minimum that has only real frequencies or a saddle point that has only one imaginary frequency. The initial state corresponding to two **1**s has closed shell (CS) singlet state obtained from restricted B3LYP calculations. The cycloadduct formation reactions were assumed to be started by visible light irradiation of one of **1** in the initial state. Thus, broken-symmetry unrestricted DFT B3LYP calculations performed to obtain the open-shell (OS) singlet state in each geometry formed after the irradiation. After the reaction, final [2+2] cycloadducts were formed, observed in the X-ray-crystallography. Due to its stability, the final product would have the CS singlet state, obtained from restricted B3LYP calculations.

For all the calculations, Gaussian 09 code was employed.[10]

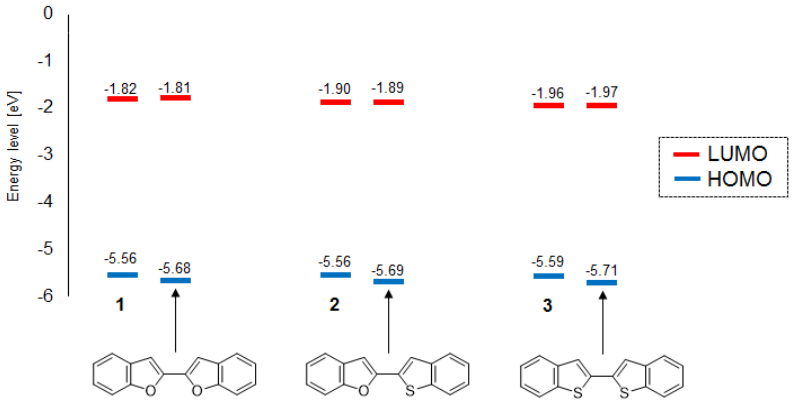


**Figure S13.** Frontier orbital energies of **1**-**3**, bibenzofuran, benzothienyl benzofuran, and bibenzothiophene estimated by DFT calculations (B3LYP/6-31G+(d,p)). The geometries of bibenzofuran, benzothienyl benzofuran, and bibenzothiophene were optimized without changing the torsion angles $E^1$−C−C−$E^2$ ($E^1$, $E^2$: O or S) from those of **1**, **2**, and **3**, respectively.

**Table S10**. Atom coordinates and absolute energy levels for **1** optimized in the $S_0$ state.

**1** ($S_0$ state): *E*(RB3LYP) = -3230.45962193 A.U.

| Center Number | Atomic Number | Atomic Type | Coordinates | | |
|---|---|---|---|---|---|
| | | | X | Y | Z |
| 1 | 6 | 0 | -0.715691 | -1.537259 | -0.159849 |
| 2 | 6 | 0 | 0.716198 | -1.537059 | -0.159931 |
| 3 | 6 | 0 | 1.32118 | -0.463763 | 0.445716 |
| 4 | 33 | 0 | 0.000032 | 0.69052 | 1.302419 |
| 5 | 6 | 0 | -1.3209 | -0.464167 | 0.445927 |
| 6 | 6 | 0 | -2.731863 | -0.693402 | 0.303519 |
| 7 | 6 | 0 | -2.842835 | -1.909442 | -0.415612 |
| 8 | 8 | 0 | -1.593067 | -2.432855 | -0.69478 |
| 9 | 8 | 0 | 1.593774 | -2.432561 | -0.6947 |
| 10 | 6 | 0 | 2.84342 | -1.908888 | -0.415536 |
| 11 | 6 | 0 | 2.732203 | -0.69279 | 0.303456 |
| 12 | 6 | 0 | -3.911045 | -0.025609 | 0.673337 |
| 13 | 6 | 0 | -5.135789 | -0.594666 | 0.330473 |
| 14 | 6 | 0 | -5.208043 | -1.809321 | -0.378874 |
| 15 | 6 | 0 | -4.051516 | -2.49293 | -0.764605 |
| 16 | 6 | 0 | 4.052226 | -2.492133 | -0.764518 |
| 17 | 6 | 0 | 5.208609 | -1.808207 | -0.378925 |
| 18 | 6 | 0 | 5.136106 | -0.593468 | 0.330255 |
| 19 | 6 | 0 | 3.911247 | -0.024649 | 0.673097 |
| 20 | 6 | 0 | -0.000359 | 2.228068 | 0.076375 |
| 21 | 6 | 0 | -0.000335 | 2.095649 | -1.316892 |
| 22 | 6 | 0 | -0.000691 | 3.22464 | -2.135968 |
| 23 | 6 | 0 | -0.001064 | 4.503026 | -1.565217 |
| 24 | 6 | 0 | -0.001067 | 4.644663 | -0.176539 |
| 25 | 6 | 0 | -0.000725 | 3.508421 | 0.641098 |
| 26 | 1 | 0 | -3.868616 | 0.913077 | 1.217072 |
| 27 | 1 | 0 | -6.055716 | -0.092044 | 0.613764 |
| 28 | 1 | 0 | -6.179039 | -2.224977 | -0.629634 |
| 29 | 1 | 0 | -4.089514 | -3.429857 | -1.309795 |
| 30 | 1 | 0 | 4.090426 | -3.429111 | -1.309605 |
| 31 | 1 | 0 | 6.179691 | -2.223679 | -0.629658 |
| 32 | 1 | 0 | 6.055932 | -0.090582 | 0.613407 |
| 33 | 1 | 0 | 3.868619 | 0.914109 | 1.216691 |
| 34 | 1 | 0 | -0.000013 | 1.106979 | -1.766905 |
| 35 | 1 | 0 | -0.000666 | 3.110068 | -3.216269 |
| 36 | 1 | 0 | -0.001367 | 5.383022 | -2.202076 |
| 37 | 1 | 0 | -0.001329 | 5.633944 | 0.272285 |
| 38 | 1 | 0 | -0.000725 | 3.624941 | 1.721995 |

**Table S11**. Atom coordinates and absolute energy levels for **2** optimized in the $S_0$ state.

**2** ($S_0$ state): *E*(RB3LYP) = -3553.44250201 A.U.

| Center Number | Atomic Number | Atomic Type | Coordinates | | |
|---|---|---|---|---|---|
| | | | X | Y | Z |
| 1 | 6 | 0 | 0.863357 | -1.467643 | 0.141605 |
| 2 | 6 | 0 | -0.569853 | -1.541742 | 0.188394 |
| 3 | 6 | 0 | -1.208306 | -0.471402 | -0.401191 |
| 4 | 33 | 0 | 0.068038 | 0.738388 | -1.27345 |
| 5 | 6 | 0 | 1.436772 | -0.384656 | -0.473562 |
| 6 | 6 | 0 | 2.855174 | -0.58525 | -0.362864 |
| 7 | 6 | 0 | 3.006232 | -1.807494 | 0.337997 |
| 8 | 8 | 0 | 1.773297 | -2.3543 | 0.643057 |
| 9 | 16 | 0 | -1.658543 | -2.736015 | 0.8539 |
| 10 | 6 | 0 | -3.040443 | -1.765232 | 0.333793 |
| 11 | 6 | 0 | -2.635884 | -0.573787 | -0.334019 |
| 12 | 6 | 0 | 4.011954 | 0.113248 | -0.745942 |
| 13 | 6 | 0 | 5.255522 | -0.435824 | -0.440023 |
| 14 | 6 | 0 | 5.36838 | -1.657533 | 0.25117 |
| 15 | 6 | 0 | 4.234446 | -2.370106 | 0.651584 |
| 16 | 6 | 0 | -4.388875 | -2.081529 | 0.521248 |
| 17 | 6 | 0 | -5.351429 | -1.198676 | 0.036451 |
| 18 | 6 | 0 | -4.972652 | -0.014731 | -0.624679 |
| 19 | 6 | 0 | -3.632981 | 0.30267 | -0.80849 |
| 20 | 6 | 0 | 0.0542 | 2.256621 | -0.02318 |
| 21 | 6 | 0 | 0.045211 | 2.100112 | 1.367627 |
| 22 | 6 | 0 | 0.04211 | 3.215451 | 2.205389 |
| 23 | 6 | 0 | 0.049747 | 4.503255 | 1.656361 |
| 24 | 6 | 0 | 0.060182 | 4.668318 | 0.270227 |
| 25 | 6 | 0 | 0.06199 | 3.546157 | -0.566527 |
| 26 | 1 | 0 | 3.938489 | 1.05893 | -1.274053 |
| 27 | 1 | 0 | 6.158495 | 0.090262 | -0.735129 |
| 28 | 1 | 0 | 6.352813 | -2.056661 | 0.474947 |
| 29 | 1 | 0 | 4.304062 | -3.31247 | 1.184266 |
| 30 | 1 | 0 | -4.681544 | -2.994395 | 1.031191 |
| 31 | 1 | 0 | -6.403998 | -1.428509 | 0.17106 |
| 32 | 1 | 0 | -5.739899 | 0.659181 | -0.993979 |
| 33 | 1 | 0 | -3.350931 | 1.221506 | -1.314349 |
| 34 | 1 | 0 | 0.040839 | 1.103752 | 1.800213 |
| 35 | 1 | 0 | 0.034169 | 3.08284 | 3.283617 |
| 36 | 1 | 0 | 0.047578 | 5.37239 | 2.307966 |
| 37 | 1 | 0 | 0.066815 | 5.665131 | -0.161631 |
| 38 | 1 | 0 | 0.069063 | 3.680532 | -1.645335 |

**Table S12**. Atom coordinates and absolute energy levels for **3** optimized in the $S_0$ state.

**3** ($S_0$ state): *E*(RB3LYP) = -3876.42314239 A.U.

| Center Number | Atomic Number | Atomic Type | Coordinates | | |
|---|---|---|---|---|---|
| | | | X | Y | Z |
| 1 | 6 | 0 | 0.721978 | -1.492885 | 0.172448 |
| 2 | 6 | 0 | -0.722397 | -1.49262 | 0.172746 |
| 3 | 6 | 0 | -1.325375 | -0.405813 | -0.419841 |
| 4 | 33 | 0 | -0.000106 | 0.771776 | -1.235898 |
| 5 | 6 | 0 | 1.325169 | -0.406295 | -0.420359 |
| 6 | 6 | 0 | 2.756554 | -0.473284 | -0.389598 |
| 7 | 6 | 0 | 3.207889 | -1.659262 | 0.256229 |
| 8 | 16 | 0 | 1.862475 | -2.666938 | 0.798302 |
| 9 | 16 | 0 | -1.863397 | -2.666638 | 0.798108 |
| 10 | 6 | 0 | -3.208301 | -1.658642 | 0.256176 |
| 11 | 6 | 0 | -2.756784 | -0.472574 | -0.38933 |
| 12 | 6 | 0 | 3.718542 | 0.433729 | -0.877752 |
| 13 | 6 | 0 | 5.070479 | 0.151474 | -0.72765 |
| 14 | 6 | 0 | 5.495405 | -1.028902 | -0.089026 |
| 15 | 6 | 0 | 4.568043 | -1.942565 | 0.407504 |
| 16 | 6 | 0 | -4.568568 | -1.941714 | 0.407411 |
| 17 | 6 | 0 | -5.495704 | -1.02778 | -0.088992 |
| 18 | 6 | 0 | -5.070541 | 0.152667 | -0.727386 |
| 19 | 6 | 0 | -3.718592 | 0.434765 | -0.87734 |
| 20 | 6 | 0 | 0.000455 | 2.26982 | 0.039341 |
| 21 | 6 | 0 | 0.000412 | 2.091098 | 1.427686 |
| 22 | 6 | 0 | 0.00075 | 3.193442 | 2.282587 |
| 23 | 6 | 0 | 0.001119 | 4.489697 | 1.753788 |
| 24 | 6 | 0 | 0.001134 | 4.676832 | 0.370414 |
| 25 | 6 | 0 | 0.00079 | 3.567827 | -0.48353 |
| 26 | 1 | 0 | 3.400141 | 1.350004 | -1.366464 |
| 27 | 1 | 0 | 5.810589 | 0.849985 | -1.106479 |
| 28 | 1 | 0 | 6.556514 | -1.232218 | 0.01875 |
| 29 | 1 | 0 | 4.896512 | -2.852685 | 0.900212 |
| 30 | 1 | 0 | -4.897293 | -2.85184 | 0.899923 |
| 31 | 1 | 0 | -6.556862 | -1.230893 | 0.018687 |
| 32 | 1 | 0 | -5.810588 | 0.85131 | -1.106098 |
| 33 | 1 | 0 | -3.399913 | 1.35107 | -1.365797 |
| 34 | 1 | 0 | 0.000111 | 1.087989 | 1.844294 |
| 35 | 1 | 0 | 0.000732 | 3.044164 | 3.35867 |
| 36 | 1 | 0 | 0.001368 | 5.34842 | 2.419071 |
| 37 | 1 | 0 | 0.001391 | 5.680358 | -0.045692 |
| 38 | 1 | 0 | 0.000788 | 3.71886 | -1.560179 |

**Table S13**. Atom coordinates and absolute energy levels for bibenzofuran optimized in the $S_0$ state fixing the torsion angle 9-8-10-14 = 0.017°.

Bibenzofuran ($S_0$ state): *E*(RB3LYP) = -766.20490227 A.U.

| Center Number | Atomic Number | Atomic Type | Coordinates | | |
|---|---|---|---|---|---|
| | | | X | Y | Z |
| 1 | 6 | 0 | 5.008813 | -1.07242 | -0.00013 |
| 2 | 6 | 0 | 5.284808 | 0.310624 | 0.000078 |
| 3 | 6 | 0 | 4.261086 | 1.25489 | 0.0002 |
| 4 | 6 | 0 | 2.93094 | 0.798057 | 0.000109 |
| 5 | 6 | 0 | 2.691714 | -0.59116 | -9.7E-05 |
| 6 | 6 | 0 | 3.696868 | -1.55015 | -0.00022 |
| 7 | 6 | 0 | 1.631467 | 1.410943 | 0.000192 |
| 8 | 6 | 0 | 0.720711 | 0.387359 | 0.000016 |
| 9 | 8 | 0 | 1.345387 | -0.84074 | -0.00015 |
| 10 | 6 | 0 | -0.72071 | 0.387359 | -1.6E-05 |
| 11 | 6 | 0 | -1.63147 | 1.410943 | -0.00019 |
| 12 | 6 | 0 | -2.93094 | 0.798057 | -0.00011 |
| 13 | 6 | 0 | -2.69171 | -0.59116 | 0.000097 |
| 14 | 8 | 0 | -1.34539 | -0.84074 | 0.000152 |
| 15 | 6 | 0 | -4.26109 | 1.25489 | -0.0002 |
| 16 | 6 | 0 | -5.28481 | 0.310624 | -7.8E-05 |
| 17 | 6 | 0 | -5.00881 | -1.07242 | 0.000128 |
| 18 | 6 | 0 | -3.69687 | -1.55015 | 0.000219 |
| 19 | 1 | 0 | 5.832121 | -1.78007 | -0.00022 |
| 20 | 1 | 0 | 6.318524 | 0.643147 | 0.000144 |
| 21 | 1 | 0 | 4.485136 | 2.317382 | 0.000359 |
| 22 | 1 | 0 | 3.467211 | -2.61011 | -0.00038 |
| 23 | 1 | 0 | 1.401282 | 2.466727 | 0.000362 |
| 24 | 1 | 0 | -1.40128 | 2.466727 | -0.00036 |
| 25 | 1 | 0 | -4.48514 | 2.317382 | -0.00036 |
| 26 | 1 | 0 | -6.31852 | 0.643146 | -0.00014 |
| 27 | 1 | 0 | -5.83212 | -1.78007 | 0.000218 |
| 28 | 1 | 0 | -3.46721 | -2.61011 | 0.000375 |

**Table S14**. Atom coordinates and absolute energy levels for benzothienyl benzofuran optimized in the $S_0$ state fixing the torsion angle 9-8-10-14 = 0.668°.

Benzothienyl benzofuran ($S_0$ state): *E*(RB3LYP) = -1089.18253855 A.U.

| Center Number | Atomic Number | Atomic Type | Coordinates | | |
|---|---|---|---|---|---|
| | | | X | Y | Z |
| 1 | 6 | 0 | 5.304698 | -0.52292 | -0.00186 |
| 2 | 6 | 0 | 5.241312 | 0.884841 | 0.004309 |
| 3 | 6 | 0 | 4.017222 | 1.540646 | 0.006996 |
| 4 | 6 | 0 | 2.82424 | 0.78845 | 0.003379 |
| 5 | 6 | 0 | 2.908757 | -0.6288 | -0.00282 |
| 6 | 6 | 0 | 4.142273 | -1.28962 | -0.00538 |
| 7 | 6 | 0 | 1.465198 | 1.244325 | 0.005438 |
| 8 | 6 | 0 | 0.547704 | 0.224745 | 0.000663 |
| 9 | 16 | 0 | 1.3164 | -1.36591 | -0.00624 |
| 10 | 6 | 0 | -0.89201 | 0.333949 | -0.00027 |
| 11 | 6 | 0 | -1.74379 | 1.406819 | -0.00685 |
| 12 | 6 | 0 | -3.07826 | 0.873022 | -0.00393 |
| 13 | 6 | 0 | -2.92539 | -0.52806 | 0.00409 |
| 14 | 8 | 0 | -1.5955 | -0.85588 | 0.006368 |
| 15 | 6 | 0 | -4.3777 | 1.410308 | -0.00756 |
| 16 | 6 | 0 | -5.45797 | 0.530763 | -0.00294 |
| 17 | 6 | 0 | -5.26761 | -0.86612 | 0.005105 |
| 18 | 6 | 0 | -3.987 | -1.42349 | 0.008774 |
| 19 | 1 | 0 | 6.271209 | -1.01782 | -0.00388 |
| 20 | 1 | 0 | 6.161567 | 1.461268 | 0.007007 |
| 21 | 1 | 0 | 3.971889 | 2.626179 | 0.01179 |
| 22 | 1 | 0 | 4.194113 | -2.37416 | -0.01006 |
| 23 | 1 | 0 | 1.1873 | 2.292386 | 0.010848 |
| 24 | 1 | 0 | -1.45317 | 2.447476 | -0.01374 |
| 25 | 1 | 0 | -4.53593 | 2.484574 | -0.01376 |
| 26 | 1 | 0 | -6.46928 | 0.926238 | -0.00558 |
| 27 | 1 | 0 | -6.1326 | -1.52218 | 0.008509 |
| 28 | 1 | 0 | -3.8236 | -2.49568 | 0.014882 |

**Table S15**. Atom coordinates and absolute energy levels for bibenzothiophene optimized in the $S_0$ state fixing the torsion angle 9-8-10-14 = 0.044°.

Bibenzothiophene ($S_0$ state): *E*(RB3LYP) = -1412.15539232 A.U.

| Center Number | Atomic Number | Atomic Type | Coordinates | | |
|---|---|---|---|---|---|
| | | | X | Y | Z |
| 1 | 6 | 0 | -5.54221 | -0.23587 | 0.000341 |
| 2 | 6 | 0 | -5.35447 | 1.160544 | -0.00082 |
| 3 | 6 | 0 | -4.07726 | 1.706077 | -0.00129 |
| 4 | 6 | 0 | -2.95502 | 0.85223 | -0.0006 |
| 5 | 6 | 0 | -3.16608 | -0.55072 | 0.000554 |
| 6 | 6 | 0 | -4.45162 | -1.10206 | 0.001033 |
| 7 | 6 | 0 | -1.56138 | 1.18797 | -0.00093 |
| 8 | 6 | 0 | -0.7271 | 0.098569 | -3.2E-05 |
| 9 | 16 | 0 | -1.64107 | -1.41806 | 0.00129 |
| 10 | 6 | 0 | 0.727097 | 0.098569 | 0.00003 |
| 11 | 6 | 0 | 1.561383 | 1.18797 | 0.000928 |
| 12 | 6 | 0 | 2.955022 | 0.852231 | 0.000596 |
| 13 | 6 | 0 | 3.166075 | -0.55072 | -0.00056 |
| 14 | 16 | 0 | 1.641069 | -1.41806 | -0.00129 |
| 15 | 6 | 0 | 4.077264 | 1.706077 | 0.001292 |
| 16 | 6 | 0 | 5.35447 | 1.160543 | 0.00082 |
| 17 | 6 | 0 | 5.542206 | -0.23587 | -0.00034 |
| 18 | 6 | 0 | 4.45162 | -1.10207 | -0.00103 |
| 19 | 1 | 0 | -6.54865 | -0.64341 | 0.000696 |
| 20 | 1 | 0 | -6.22022 | 1.816067 | -0.00135 |
| 21 | 1 | 0 | -3.93689 | 2.783455 | -0.00219 |
| 22 | 1 | 0 | -4.59807 | -2.17788 | 0.001919 |
| 23 | 1 | 0 | -1.20067 | 2.210191 | -0.00194 |
| 24 | 1 | 0 | 1.200667 | 2.210192 | 0.001932 |
| 25 | 1 | 0 | 3.936889 | 2.783455 | 0.002185 |
| 26 | 1 | 0 | 6.22022 | 1.816067 | 0.001348 |
| 27 | 1 | 0 | 6.548648 | -0.64341 | -0.00069 |
| 28 | 1 | 0 | 4.598069 | -2.17788 | -0.00192 |

## 12. Mechanism of [2+2] cycloaddition of 1

To understand the formation of [2+2] cycloadduct (Chart S1) obtained in the X-ray crystallography (Table S7), DFT B3LYP calculations with the 6-31G(d,p) basis set were performed. Since [2+2] cycloadditions are prohibited in thermal reactions based on fundamental organic chemistry,[11] the formation reaction was assumed to be initiated by irradiation of **1** by visible light, followed the discussion in the main text (Fig. 3). Once the excited state of **1** (the open-shell (OS) singlet state) is generated, it can bind another molecule of **1** in the ground state (closed-shell (CS) singlet state) to form an initial adduct in the OS singlet state. Considering amplitude distributions of orbitals contributing the electronic transition in Fig. 3, carbon atoms on the arsole ring would be more reactive in the OS single state toward another molecule of **1**. In reference to Ref. S11, two [2+2] cycloadducts are conceivable; *anti* and *syn* [2+2] cycloadducts, which are depicted in Scheme S1.

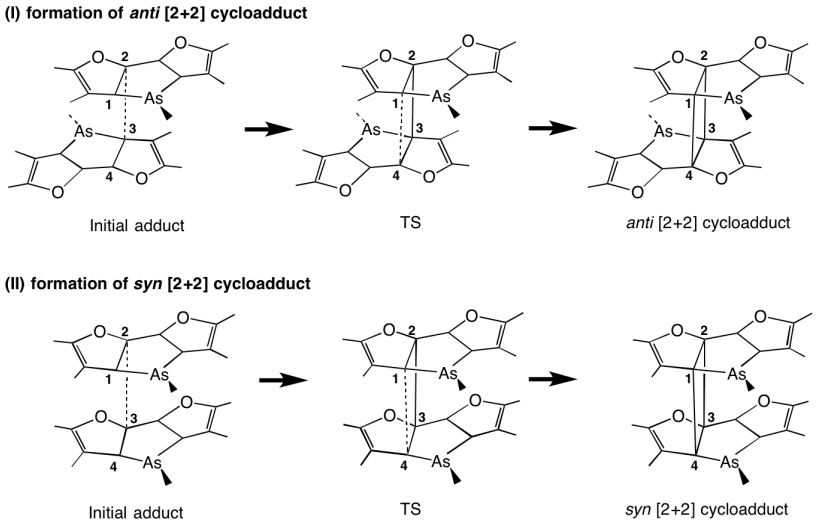


**Scheme S1.** Formation of anti and *syn* [2+2] cycloadducts.

To discuss in detail the formation of *anti* and *syn* [2+2] cycloadducts from visible-light-induced dimerization of **1**, their local minima and transition states were investigated. In fact, the optimized geometries for the initial adducts and transition states in the OS single states,[12] as well as the [2+2] cycloadducts in the CS single states were obtained in Figure S14.[13] Detailed information in the optimized geometries are listed in Tables S16 and S17. Their energetics relative to two **1** molecules in the CS single states (initial states) are also displayed in Figure S14. Note that the broken-symmetry methodology was used to obtain the OS single states. Judging from spin densities in Tables S16 and S17, OS systems in the initial adducts and transitions states were successfully obtained.

As shown in Figure S14, each initial adduct has two carbon atoms between which a covalent bond is being formed in two **1** molecules; see the *L*(2−3) values in Tables S16 and S17. After the formation of the initial adduct, two carbon atoms labeled by 1 and 4 approach each other to form another covalent bond in TS, leading to the four-membered ring in the [2+2] cycloadduct. Considering the energy diagrams in Figure S14, visible-light irradiation is indispensable to proceed the [2+2] cycloaddition reaction, because the energy difference between TS and the initial state (> 40 kcal/mol) cannot be overcome in thermal conditions. In addition, DFT calculations found the formation of *syn* [2+2] cycloadduct is slightly favorable rather than that of *anti* [2+2] cycloadduct, by comparing the two reactions pathways in terms of the activation energy ($E_a$) values. However, the *anti* [2+2] cycloadduct was only observed in X-ray crystallography. This discrepancy indicates that the formation of [2+2] cycloadducts is thermodynamically controlled rather than kinetically. In fact, the *anti* [2+2] cycloadduct is more stable than the initial state by 2.5 kcal/mol, which can explain the presence of the *anti* [2+2] cycloadduct in X-ray crystallography, although the majority is the monomeric form of **1**. Furthermore, the *syn* [2+2] cycloadduct is energetically identical to the initial state, and thus photo-irradiated reactions to form *syn* [2+2] cycloadduct is not needed, instead, in this situation, the monomeric form of **1** can exist.

**Table S16.** Information of optimized geometries formed in the reaction to form the *anti* [2+2] cycloadduct, obtained from the B3LYP/6-31G** level of theory.

| | *L*(1−2)[2] | *L*(2−3)[2] | *L*(3−4)[2] | *L*(1−4)[2] | S(1)[3] | S(2)[3] | S(3)[3] | S(4)[3] |
|---|---|---|---|---|---|---|---|---|
| Initial adduct[1] | 1.49 | 1.65 | 1.50 | 3.07 | 0.51 | −0.10 | 0.09 | −0.62 |
| TS[1] | 1.52 | 1.59 | 1.53 | 2.63 | 0.58 | -0.08 | 0.07 | −0.67 |
| [2+2]cycloadduct [1] | 1.57 | 1.58 | 1.57 | 1.57 | 0 | 0 | 0 | 0 |

[1] Optimized geometries labels: see in Figure S14.

[2] *L*(*n*−*m*): optimized internuclear separation between carbon atoms labeled by *n* and *m*

[3] *S*(*n*): spin density on the carbon atom labeled by *n*.

**Table S17.** Information of optimized geometries formed in the reaction to form the *syn* [2+2] cycloadduct, obtained from the B3LYP/6-31G** level of theory.

| | $L(1-2)^2$ | $L(2-3)^2$ | $L(3-4)^2$ | $L(1-4)^2$ | $S(1)^3$ | $S(2)^3$ | $S(3)^3$ | $S(4)^3$ |
|---|---|---|---|---|---|---|---|---|
| Initial adduct[1] | 1.50 | 1.64 | 1.50 | 3.03 | −0.62 | 0.09 | −0.09 | 0.62 |
| TS[1] | 1.54 | 1.58 | 1.53 | 2.60 | −0.64 | 0.07 | −0.07 | 0.64 |
| [2+2]cycloadduct [1] | 1.57 | 1.58 | 1.57 | 1.59 | 0 | 0 | 0 | 0 |

[1] Optimized geometries labels: see in Figure S14.

[2] $L(n-m)$: optimized internuclear separation between carbon atoms labeled by $n$ and $m$

[3] $S(n)$: spin density on the carbon atom labeled by $n$.

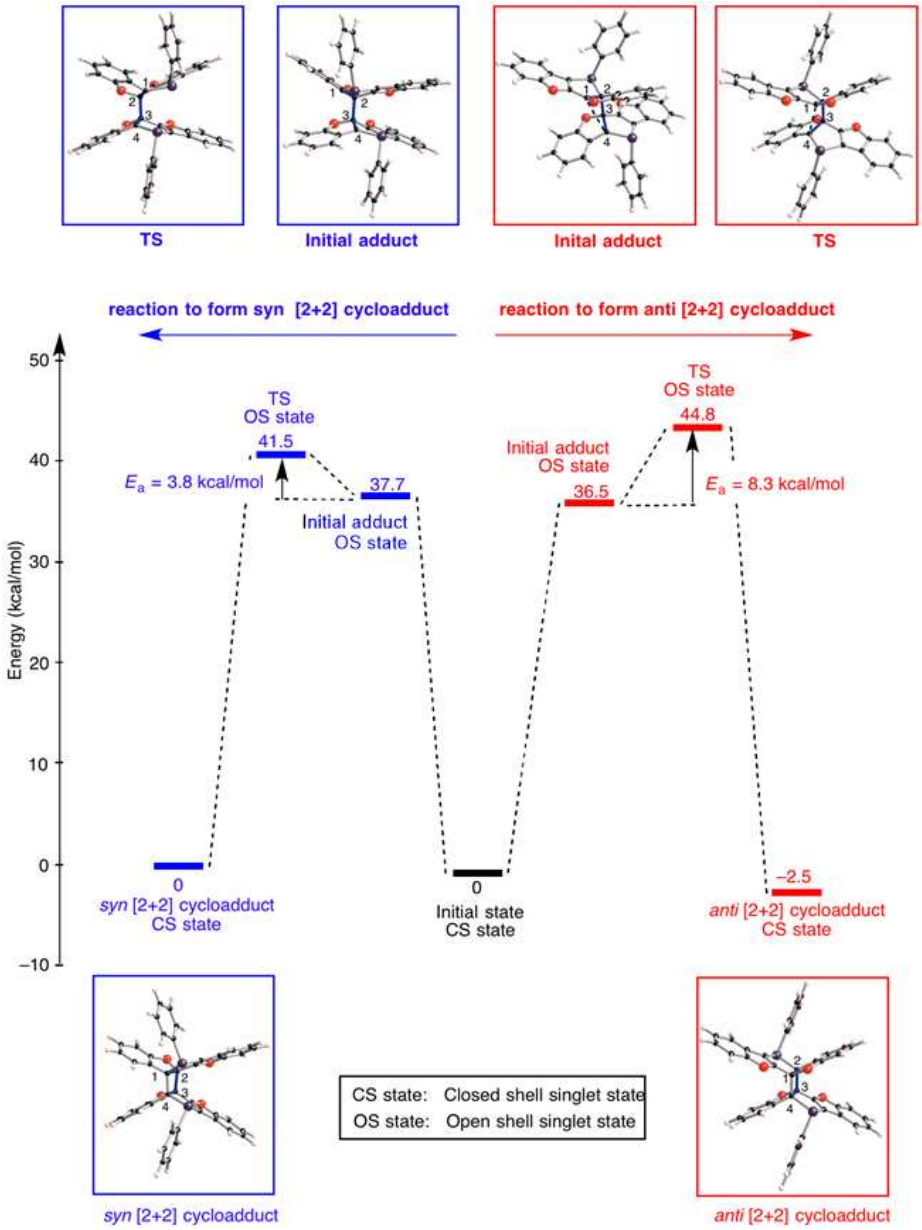


**Figure S14.** Potential energy surfaces (PES) of the formation of [2+2] cycloadducts by dimerization of 1 induced by visible-light irradiation of **1**. Local minima and the transition state in the formation of syn and anti cycloadducts are given by blue and red colors, respectively.

## 13. Reference


(1) Kato, T.; Tanaka, S.; Naka, K. *Chem. Lett*. **2015**, *44*, 1476-1478.
(2) Mehta, S.; Larock, R. C. *J. Org. Chem.* **2010**, *75*, 1652-1658.
(3) Oechsle, P.; Paradies, J. *Org. Lett.* **2014**, *16*, 4086-4089.
(4) CrystalClear: Data Collection and Processing Software, Rigaku Corporation (1998-2014). Tokyo 196-8666, Japan.
(5) *SIR2011*: M. C. Burla, R. Caliandro, M. Camalli, B. Carrozzini, G. L. Cascarano, C. Giacovazzo, M. Mallamo, A. Mazzone, G. Polidori, R. J. Spagna, *Appl. Cryst.* **2012**, *45*, 357.
(6) *CrystalStructure 4.1*: Crystal Structure Analysis Package, Rigaku Corporation (2000-2014). Tokyo 196-8666, Japan.
(7) *SHELXL2013*: G. M. Sheldrick, *Acta Cryst*. **2008**, *A64*, 112.
(8) Fleming, I. Ed., *Science of Synthesis Category 1, vol 4*; G. Thieme: Stuttgart, Germany 2002; Chapter 4.1, pp 13.
(9) To understand the mechanism of the [2+2] cycloaddition of **1**, we conducted some experiments in which solutions of **1** were subjected to photo-irradiation. However, compound **1** is not sufficiently stable under such conditions; deep yellow-colored complex mixtures were obtained after these reactions. Therefore, we conducted computational studies to understand the reaction mechanism.
(10) Gaussian 09, Revision C.01, Frisch, M. J.; Trucks, G. W.; Schlegel, H. B.; Scuseria, G. E.; Robb, M. A.; Cheeseman, J. R.; Scalmani, G.; Barone, V.; Mennucci, B.; Petersson, G. A.; Nakatsuji, H.; Caricato, M.; Li, X.; Hratchian, H. P.; Izmaylov, A. F.; Bloino, J.; Zheng, G.; Sonnenberg, J. L.; Hada, M.; Ehara, M.; Toyota, K.; Fukuda, R.; Hasegawa, J.; Ishida, M.; Nakajima, T.; Honda, Y.; Kitao, O.; Nakai, H.; Vreven, T.; Montgomery, J. A., Jr.; Peralta, J. E.; Ogliaro, F.; Bearpark, M.; Heyd, J. J.; Brothers, E.; Kudin, K. N.; Staroverov, V. N.; Kobayashi, R.; Normand, J.; Raghavachari, K.; Rendell, A.; Burant, J. C.; Iyengar, S. S.; Tomasi, J.; Cossi, M.; Rega, N.; Millam, M. J.; Klene, M.; Knox, J. E.; Cross, J. B.; Bakken, V.; Adamo, C.; Jaramillo, J.; Gomperts, R.; Stratmann, R. E.; Yazyev, O.; Austin, A. J.; Cammi, R.; Pomelli, C.; Ochterski, J. W.; Martin, R. L.; Morokuma, K.; Zakrzewski, V. G.; Voth, G. A.; Salvador, P.; Dannenberg, J. J.; Dapprich, S.; Daniels, A. D.; Farkas, Ö.; Foresman, J. B.; Ortiz, J. V.; Cioslowski, J.; Fox, D. J. Gaussian, Inc., Wallingford CT, 2009.
(11) Clayden, J.; Greeves, N.; Warren, S.; Wothers, P. *Organic Chemistry* 2001 Oxford University Press.
(12) The OS single state is assumed to correspond to the excited state formed by the photo-irradiation.
(13) We confirmed that transition states have one imaginary mode, where carbon atoms labelled by 1 and 4 approach each other to form a covalent bond (61 $i$cm$^{-1}$ for the pathway for *anti* [2+2] cycloadduct and 94 $i$cm$^{-1}$ for *syn* [2+2] cycloadduct), and local minima do not have imaginary mode.